Research in Astron. Astrophys. **2010** Vol. **10** No. **6**, 533–540
http://www.raa-journal.org *http://www.iop.org/journals/raa*

Research in Astronomy and Astrophysics

Not enough evidence to support the correlation between gamma-ray bursts and foreground galaxy clusters in the *Swift* Era *

Jing Wang and Jian-Yan Wei

National Astronomical Observatories, Chinese Academy of Sciences, Beijing 100012, China; *wj@bao.ac.cn*

Received 2010 January 21; accepted 2010 March 26

Abstract The correlation between distant Gamma-Ray Bursts (GRBs) and foreground galaxy clusters is re-examined by using the well localized (with an accuracy down to a few arcsec) *Swift*/XRT GRBs. The galaxy clusters are compiled from both the X-ray selected *ROSAT* brightest cluster sample (BCS) and the BCS extension by requiring $\delta \geq 0^\circ$ and $b \geq 20^\circ$. The *Swift*/XRT GRBs fulfilling the above selection criteria are cross-correlated with the clusters. Both Nearest-Neighbor analysis and the angular two-point cross-correlation function show that there is not enough evidence supporting the correlation between the GRBs and foreground clusters. We suggest that the non-correlation is probably related to the GRB number-flux relation slope.

Key words: gamma rays: bursts — galaxies: clusters: general — methods: statistical

1 INTRODUCTION

There is now no doubt that Gamma-Ray Bursts (GRBs) take place at cosmological distances. Thanks to the prompt locating ability and deep follow-up observations, the record of the highest redshift of GRBs has been progressively broken in the past a few years, especially after the launch of the *Swift* satellite (Gehrels et al. 2004). At present, GRB 090423 detected by the *Swift* satellite is the most distant GRB with a redshift of ~ 8.1 (Salvaterra et al. 2009). So far, there are about 50 *Swift* detected GRBs with measured redshifts. A majority of these GRBs lie beyond $z = 1$ with a redshift distribution that peaks at $z \sim 1 - 2$.

The cosmological origin and high luminosities offer an opportunity to use GRBs as tracers to study the following topics: the star formation history of the Universe (e.g., Savaglio et al. 2009; Jakobsson et al. 2005); the properties and evolution of the intergalactic medium and high redshift galaxies (e.g., Prochaska et al. 2006; Prochter et al. 2006; Vergani et al. 2009), similar to that done with the high redshift quasars; and the nearby mass distribution through the weak lensing of GRBs caused by the local large-scale structure (Williams & Frey 2003 and references therein).

Because GRBs are point-like sources, their weak lensing could only be detected through the angular correlation between sources and corresponding lenses[1]. A number of authors have previously

* Supported by the National Natural Science Foundation of China.

[1] Another way of looking for candidates that show the GRB lensing effect is based on the time delay of two bursts from the same sky region (e.g., Veres et al. 2009)

examined whether subsets of GRBs are correlated with subsets of foreground galaxy clusters. The results obtained by these authors are, however, contradictious. Kolatt & Piran (1996) claimed that the 136 GRBs selected from the Burst and Transient Source Experiment (BATSE) 3B catalog are correlated with the Abell cluster (Abell et al. 1989) within an angular separation of 4° at a significance level of 95%. Marani et al. (1997) obtained a stronger correlation by using the BATSE GRBs with more accurate positions. By contrast, Hurley et al. (1999) did not find any evidence for the correlation between GRBs and galaxy clusters by extending the GRB sample to the BATSE 4B/Third Interplanetary Network catalog. In addition, Williams & Frey (2003) reported an anti-correlation between the BATSE GRBs and Abell clusters.

A caveat in these previous studies is the large BATSE error box that usually ranges from a fraction of a degree to a few degrees. The error box in some cases is as high as $\sim 30^\circ$. The poor localization has been greatly improved after the launch of the *Swift* satellite. The *Swift* satellite can quickly slew to the GRB position given by the BAT instrument within 100 s. Due to its high sensitivity, the XRT onboard the *Swift* satellite has the capability to measure the X-ray afterglow position with an accuracy better than $5''$ within 100 s for about 90 percent of BAT triggers (Burrows et al. 2005).

Here, we re-examine the correlation between GRBs and foreground galaxy clusters by using the *Swift*/XRT sample. As mentioned above, the highly accurate positioning ability provided by the XRT instrument allows us to regard these GRBs as point sources. The correlation is studied by the nearest-neighbor distance method and angular two-point cross-correlation function. Both methods indicate that there is no significant correlation between the GRBs and foreground galaxy clusters. The paper is organized as follows. Section 2 describes the sample selection. The analysis and results are presented in Section 3. A short discussion and conclusions are provided in Section 4.

2 SAMPLE SELECTION

The correlation between GRBs and foreground galaxy clusters is investigated in the current study by using both an X-ray selected *ROSAT* brightest cluster sample (BCS, Ebeling et al. 1998) and the BCS extension (Ebeling et al. 2000). Both samples are selected from the *ROSAT* All-Sky Survey (RASS) in the northern hemisphere ($\delta \geq 0^\circ$) and at high Galactic latitudes ($|b| \geq 20^\circ$). By combining the two samples, the completeness is about 75% down to a total flux limit of 2.8×10^{-12} erg s^{-1} cm^{-2}. There are totally 203 and 107 clusters in the BCS and BCS extension, respectively. Among the combined sample, 300 clusters have measured redshifts less than 0.3 (see fig. 3 in Ebeling et al. 2000). The *Swift*/XRT GRBs are selected from the current *Swift*/XRT catalog [2].

To test the association of GRBs with foreground galaxy clusters, we further select a subset of GRBs and a subset of clusters from the selected samples given above by requiring $\delta \geq 0^\circ$ and $b \geq 20^\circ$. Our samples used in this study are finally comprised of 116 *Swift*/XRT detected GRBs (hereafter GRB sample for short) and 223 clusters. A sub-sample of 54 GRBs (hereafter GRBz sample) with measured redshifts (both spectroscopic and photometric redshifts) is extracted from the GRB sample. Figure 1 shows the distributions of the GRBs and clusters on the sky in equatorial coordinates. The total sky area covered by the cluster sample and by the GRB sample is calculated to be 9684 square degrees.

Figure 2 shows the redshift distribution of the GRBs listed in the GRBz sample. Note that all the GRBs have redshifts larger than 0.3, which differs greatly from the redshift distribution of the clusters, except for two outliers: GRB 060502B (at $z = 0.287$) and GRB 050509B (at $z = 0.225$). The comparison of the redshift distributions between the GRBs and clusters indicates that the relation between the GRBs and clusters, if any, is unlikely to be affected by their physical association. In fact, our Nearest-Neighbor Analysis (NNA, see below) shows that the redshifts of the closest

[2] The catalog can be obtained from the web site *http://heasarc.gsfc.nasa.gov/docs/swift/archive/grb_table/.*

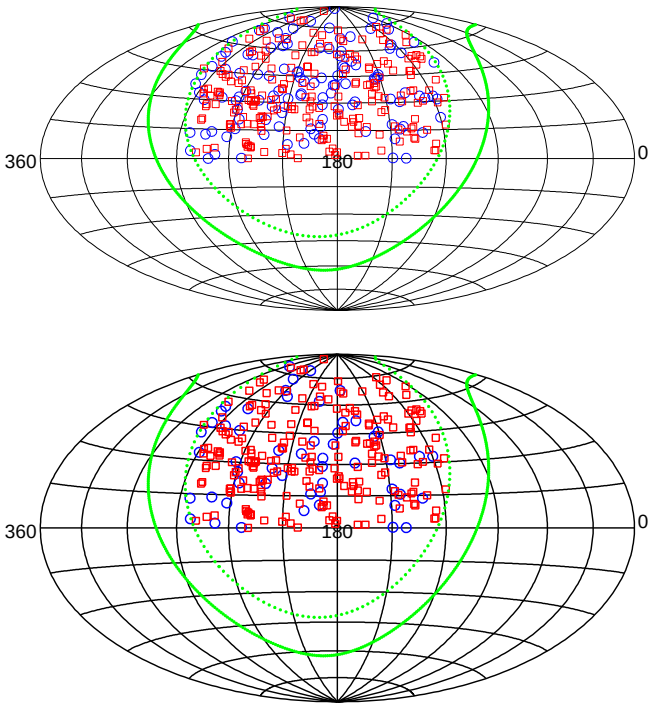

Fig. 1 Distributions of the samples used in this study on the sky in the equatorial coordinate system. The GRBs are marked by the blue open circles. The upper and lower panels show the GRB sample and GRBz sample, respectively. The solid and open red squares present the used foreground clusters listed in the BCS and BCS extension, respectively. The equatorial plane of the Galactic coordinates and the plane with a Galactic latitude of $b = 20^{\circ}$ are marked by green solid and green dotted lines, respectively.

clusters associated with GRB 060502B and GRB 050509B are 0.0473 (Zwicky 8338) and 0.1997 (Abell 1602), respectively.

3 ANALYSIS AND RESULTS

In this section, we re-examine the correlation between GRBs and foreground galaxy clusters in terms of the samples established in the above section. Both NNA and an angular two-point correlation function are adopted in our analysis.

3.1 Nearest-Neighbor Analysis

NNA is believed to be insensitive to the inhomogeneous distribution of samples on large scales. It has been widely used in searching for anisotropies in astronomy (e.g., Bahcall & Soneira 1981; Impey & He 1986; Yang et al. 1995; Mészáros & Štoček 2003). The main advantage of NNA is its simplicity in that the method uses only $2N$ angular distances (pairs). In addition to the simplicity, the nearest-neighbor distance directly reflects the association of two types of objects. The null hypotheses of the NNA is that both GRBs and clusters are uniformly distributed on the sky according to Poisson statistics. The hypotheses mean that the probability of finding the nearest neighbor in the range between θ and $\theta + d\theta$ can be described by the following probability density function which was

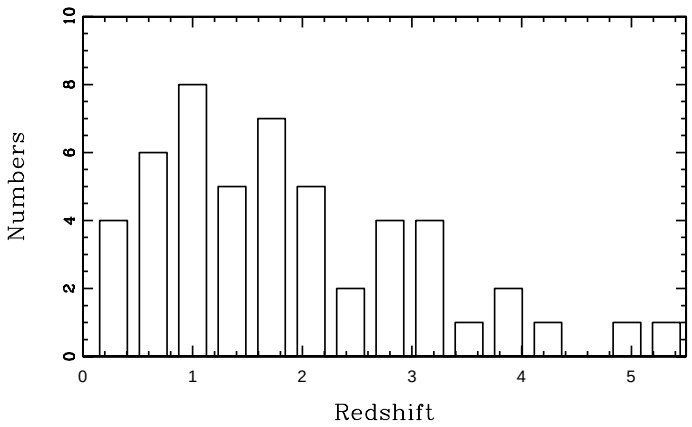

Fig. 2 Redshift distribution of the 54 *Swift*/XRT GRBs used in this study.

rigorously derived in Scott & Tout (1989):

$$P(\theta)d\theta = 2\pi n\theta e^{-\pi n\theta^2}d\theta, \tag{1}$$

where n is the surface density of the objects.

The solid line shown in each panel of Figure 3 plots the calculated empirical distribution of the nearest-neighbor distances. The distributions are plotted by binning the data into an angular bin size of 1°. The left column shows the distributions of the nearest-neighbor distances of the clusters, GRB sample, and GRBz sample. The right column shows the distributions of distance between the clusters and the GRB sample, and distance between the clusters and GRBz sample. Each empirical distribution is compared with a simulated distribution shown by the heavy dashed line. Each simulated distribution is obtained through 500 random experiments of GRB/cluster distributions on the sky, and binned into the same angular bin size. Every random sample not only has the same amount of real data, but also the same sky coverage. The two sets of thin dashed lines in each panel mark the 1σ and 2.5σ confidence limits derived from the simulation by assuming a Gaussian distribution. The Gaussian distribution is, however, no longer a good approximation when only a small number of events are detected. In these cases (typically, fewer than 10 events), the error tables given in Gehrels (1986) are adopted here to provide reasonable limits.

Clearly, one can see that all the empirical distributions are very consistent with the expected distributions if the GRBs and clusters are randomly distributed, except for the case of the clusters (see the upper-left panel in Fig. 3). There is a significant clustering (with a significance level larger than 99%) for the clusters when the angular distance between two clusters is less than 3°, although the clusters become more randomly distributed over the sky on larger scales. In fact, this significant clustering is well confirmed by our subsequent analysis based upon a two-point correlation function (see Fig. 4). This result is also qualitatively in agreement with the previous studies (e.g., Zandivarez et al. 2001; Bahcall & West 1992; Croft et al. 1997).

3.2 Angular Two-point Correlation Function

The two-point correlation function is a commonly used statistical tool for researching the large scale structure. The angular two-point correlation function $\omega(\theta)$ is defined as the probability of finding an object in a solid angular element $d\Omega$ at an angular distance θ from another given object:

$$dP = n[1 + \omega(\theta)]d\Omega, \tag{2}$$

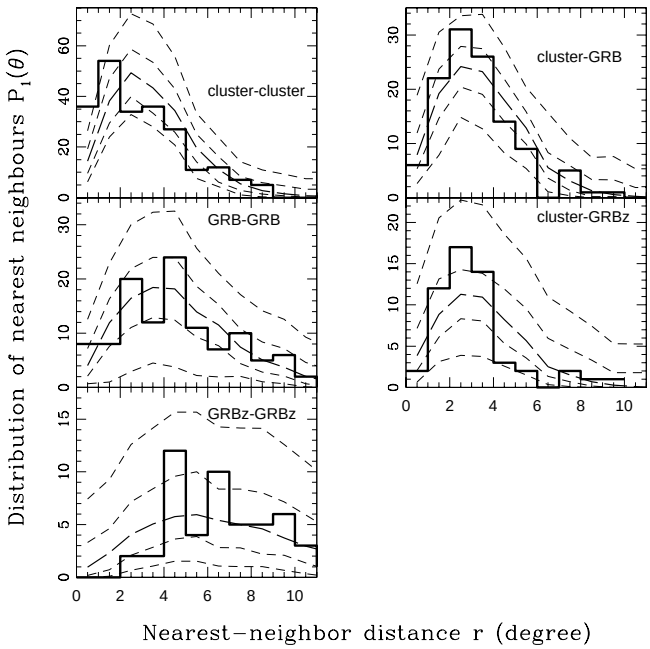

Fig. 3 Calculated empirical distributions of the nearest-neighbor distances are compared with Monte-Carlo simulations with 500 random experiments. The left column shows the distributions of the nearest-neighbor distances of the clusters, GRB sample, and the GRBz sample. The right column shows the distributions of distance between the clusters and the GRB sample, and distance between the clusters and the GRBz sample. In each panel, the calculated empirical distribution of the nearest-neighbor distance is presented by the solid line, and the Monte-Carlo simulation by the dashed lines. The two sets of the thin dashed lines in each panel mark the 1σ and 2.5σ confidence limits derived from the simulation.

where n is the mean surface density of the objects in the sample. We calculate the auto-correlation function by the natural estimator:

$$1 + \omega(\theta) = \frac{DD(\theta)}{RR(\theta)}, \tag{3}$$

where DD and RR are the numbers of data-data and random-random pairs, respectively, at an angular distance θ. The cross-correlation function is calculated by the simple estimator proposed by Peebles (1980):

$$1 + \omega(\theta) = \frac{D_1 D_2(\theta)}{D_1 R_2(\theta)}, \tag{4}$$

where $D_1 D_2$ is the number of cluster-GRB(z) pairs at an angular distance θ, and $D_1 R_1$ the number of cluster-random pairs at the same angular distance.

Generally, a positive two-point correlation function means some association, and a negative function some avoidance. If the objects are uniformly distributed, the function will be zero. The calculated auto-correlation functions are shown in the left column in Figure 4, and the cross-correlation function in the right column. A Monte-Carlo simulation with 500 random experiments is performed to calculate each two-point correlation function and its corresponding significance level. The random catalogs are generalized by the same method used in NNA. All the functions are obtained by binning the data into an angular bin size of 1°. As was the case previously reported for the NNA,

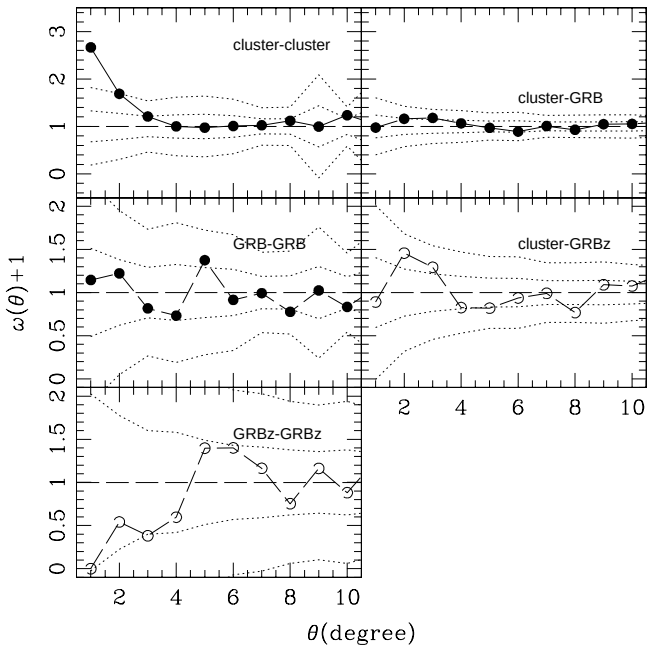

Fig. 4 Left and right columns present the auto-correlation functions and cross-correlation functions, respectively. All the functions are binned into a bin size of 1°. In each panel, the calculated empirical two-point correlation function is presented by the solid (or dashed) line. The two sets of thin dotted lines in each panel mark the 1σ and 2.5σ confidence limits derived from the Monte-Carlo simulation with 500 random experiments.

no correlation between the clusters and the GRB (GRBz) sample can be significantly identified in our current study. A significant result can only be identified for the auto-correlation function of the clusters (with a significance level $> 90\%$). The clusters are clustered at small angular distance scales $\theta < 3^\circ$.

4 CONCLUSIONS AND IMPLICATION

With much improved burst locations down to a few arcseconds, the *Swift*/XRT GRB sample allows us to re-examine the correlation between GRBs and foreground galaxy clusters. By using the NNA and angular two-point cross-correlation function, our analysis indicates that there is not enough evidence supporting the correlation between the foreground X-ray selected *ROSAT* brightest clusters and *Swift*/XRT GRBs.

Although our study is not the first one examining the relation between GRBs and foreground galaxy clusters, it is indeed the first study using the GRBs' position information with an accuracy down to a few arcseconds. The contradiction with the results obtained before 2004 (see more details and the references listed in Sect. 1) is likely due to the poor localization of the BATSE GRB sample. It is noted that the error boxes of the BATSE GRBs range from a fraction of a degree to as large as $\sim 30^\circ$.

Generally speaking, the motivation for searching for a correlation between distant GRBs and nearby massive structures is to study the local large structure in terms of the weak lensing effect of the GRBs. Assuming that the weak lensing effect indeed occurs for the GRBs, how can we understand the non-correlation revealed in the current study? In fact, the association due to the weak lensing

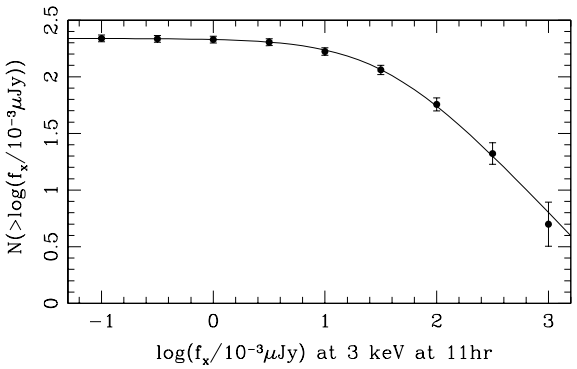

Fig. 5 Number-flux relation for the GRBs compiled by Zheng et al. (2009). The data are evenly binned into 9 bins in logarithmic space. The over-plotted error bars are 1σ Poisson noise. The solid line is the best fitted smoothed power law model (see Eq. (6)).

effect not only depends on the mass of the lenses, but also depends on the number-flux relation of the background objects. Weak lensing not only increases the brightness of faint objects, but it also expands the area behind the lenses. Combining these two competing factors, the correlation function could be related to the number-flux relation by (e.g., Williams & Irwin 1998; Myers et al. 2003)

$$\omega(\theta) = \mu^{2.5\beta-1} - 1, \tag{5}$$

where the number-flux relation is approximately described as a power law: $N(> \log f) \propto 10^{-2.5\beta \log f}$ (Boyle et al. 1988); μ is the magnification factor. This equation indicates that $\omega(\theta) = 0$ when $\beta = 0.4$.

The value of β can be constrained from the *Swift*/XRT observations. To estimate β, we use the sample recently compiled by Zheng et al. (2009). Zheng et al. (2009) collected the information about the amount of GRBs observed by the *Swift* satellite before 2008 from the literature and online databases. The number-flux relation of these GRBs is displayed in Figure 5 for the 3 keV X-ray flux density at 11 h. The data are evenly binned into 9 bins in logarithmic space. The over-plotted error bars correspond to the 1σ Poisson noise in each bin. The solid line plots the best fitted smoothed power law model with the expression:

$$\frac{dN}{d\log f} = \frac{N_0}{10^{a(\log f - \log f_0)} + 10^{b(\log f - \log f_0)}}, \tag{6}$$

where $N_0 = 218$ is the total number of GRBs. Comparing the equation with Equation (5) yields $\beta = 0.4b$ at the bright end. A weighted least-squares fitting yields the following parameters: $a = -0.0003 \pm 0.003$, $b = 1.05 \pm 0.03$, and $\log f_0 = 1.55 \pm 0.02$. Although the sample seems to clearly be incomplete at the faint end, β is inferred to be 0.42 ± 0.01 from the well sampled bright end. In fact, about half of the GRBs listed in the GRB sample are bright in X-ray with $\log(f_x/10^{-3}\mu\mathrm{Jy}) > 1.5$. This exercise suggests that the zero correlation function of the GRBs is likely due to their number-flux relation, although the weak lensing effect may indeed occur for these GRBs.

Acknowledgements We are grateful to Professor Z. G. Deng for discussions and suggestions about the statistics used in this paper. The authors thank the anonymous referee for comments and suggestions that improved the paper. This work was funded by the National Natural Science Foundation of China (Grant No. 10803008) and the National Basic Research Program of China (Grant 2009CB824800), and supported by the Chinese Academy of Sciences (Grant KJCXZ-YW-T19).

References

Abell, G. O., Corwin, H. G. Jr., & Olowin, R. P. 1989, ApJS, 70, 1
Bahcall, J. N., & Soneira, R. M. 1981, ApJ, 246, 122
Bahcall, N. A., & West, M. J. 1992, ApJ, 392, 419
Boyle, B. J., Fong, R., & Shanks, T. 1988, MNRAS, 231, 897
Burrows, D. N., Hill, J. E., Nousek, J. A., et al. 2005, Space Science Reviews, 120, 165
Croft, R. A. C., Dalton, G. B., Efstathiou, G., et al. 1997, MNRAS, 291, 305
Ebeling, H., Edge, A. C., Bohringer, H., et al. 1998, MNRAS, 301, 881
Ebeling, H., Edge, A. C., Allen, S. W., et al. 2000, MNRAS, 318, 333
Gehrels, N. 1986, ApJ, 303, 336
Gehrels, N., Chincarini, G., Giommi, P., et al. 2004, ApJ, 611, 1005
Hurley, K., Hartmann, D. H., Kouveliotou, C., et al., 1999, ApJ, 515, 497
Impey, C. D., & He, X. -T. 1986, MNRAS, 221, 897
Jakobsson, P., Bjornsson, G., Fynbo, J. P. U., et al. 2005, MNRAS, 362, 245
Kolatt, T., & Piran, T. 1996, ApJ, 467, L41
Marani, G. F., Nemiroff, R. J., Norris, J. P., et al. 1997, ApJ, 474, 576
Mészáros, A., & Štoček, J. 2003, A&A, 403, 443
Myers, A. D., Outram, P. J., Shanks, T., et al. 2003, MNRAS, 342, 467
Peebles, P. J. E. 1980, The Large Scale Structure in the Universe (Princeton: Princeton Univ. Press)
Prochaska, J. X., Bloom, J. S., Chen, H. -W., et al. 2006, ApJ, 642, 989
Prochter, G. E., Prochaska, J. X., Chen, H. -W., et al. 2006, ApJ, 648, L93
Salvaterra, R., Della Valle, M., Campana, S., et al. 2009, Nature, 461, 1258
Savaglio, S., Glazebrook, K., & Le Borgne, D. 2009, ApJ, 691, 182
Scott, D., & Tout, C. A. 1989, MNRAS, 241, 109
Veres, P., Bagoly, Z., Mészáros, A., et al. 2009, astro-ph/arXiv0912.3928
Vergani, S. D., Petitjean, P., Ledoux, C., et al. 2009, A&A, 503, 771
Williams, L. L. R., & Frey, N. 2003, ApJ, 583, 594
Williams, L. L. R., & Irwin, M. 1998, MNRAS, 298, 378
Yang, Z. L., He, X. T., & Liang, K. 1995, AJ, 109, 56
Zandivarez, A., Abadi, M. G., & Lambas, D. G. 2001, MNRAS, 326, 147
Zheng, W. K., Deng, J. S., & Wang, J. 2009, RAA (Research in Astronomy and Astrophysics), 9, 1103